General Disclaimer

One or more of the Following Statements may affect this Document

- This document has been reproduced from the best copy furnished by the organizational source. It is being released in the interest of making available as much information as possible.

- This document may contain data, which exceeds the sheet parameters. It was furnished in this condition by the organizational source and is the best copy available.

- This document may contain tone-on-tone or color graphs, charts and/or pictures, which have been reproduced in black and white.

- This document is paginated as submitted by the original source.

- Portions of this document are not fully legible due to the historical nature of some of the material. However, it is the best reproduction available from the original submission.

UNIVERSITY OF HAWAII

INSTITUTE FOR ASTRONOMY
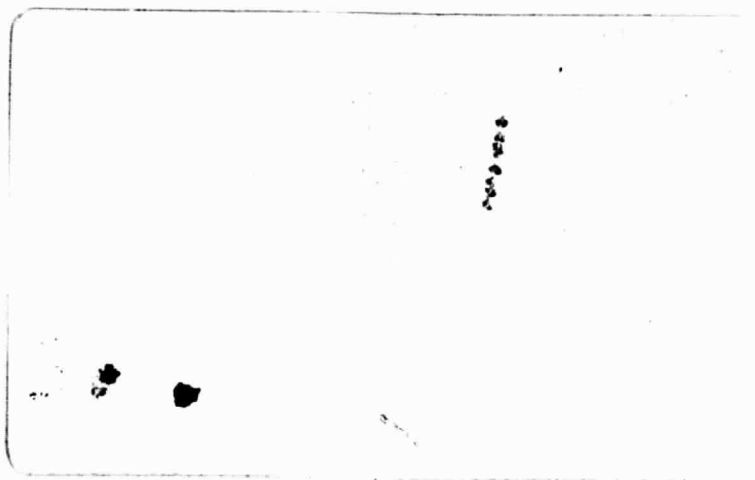
DETERMINATION OF THE IO HEAT FLOW, I:

ECLIPSE OBSERVATIONS

William M. Sinton* and Charles Kaminski

Institute for Astronomy
University of Hawaii
Honolulu, Hawaii 96822

Pages: 27
Figures: 5
Tables: 8

Running head: Io Eclipse Observations

Editorial Correspondence: Louise Good, Publications Editor
                           Institute for Astronomy
                           2680 Woodlawn Drive
                           Honolulu, HI 96822

ABSTRACT

We report 1981-1982 thermal infrared observations of five Io eclipse reappearances and one eclipse disappearance. Absolute calibration errors were estimated from measurements of Callisto during four of the eclipses with the following values: 10% at 8.7, 10.2, 12.5, and 20 μm; and 15% at 30 μm. The subsolar temperature determined for Callisto at 5.42-5.44 AU from the Sun was 168.5° K, which is in reasonable agreement with predictions using the solar constant.

We compare our observations to those of Morrison and Telesco (1980) and find that the Io flux just before emergence from eclipse is within 10% of the 1980 measurement at 10 μm. Our preemergence 20-μm measurements are in good agreement with those of Morrison and Telesco.

At 4.8 μm we find, from differencing sunlit and nonsunlit Io measurements, albedos of 0.69 ± 0.02 and 0.60 ± 0.05 at orbital phase angles of 17° and 343°, respectively. These albedos, at a solar phase angle ~9°, are free from contributions by the thermal emission of the volcanoes. When they are compared to the "albedos" determined from the monitoring program (Sinton et al., 1983) they are significantly lower than all but a few of these measurements. The difference is the thermal emission of the volcanoes which occurs almost all of the time.

Lastly, we point out a substantial disagreement between observations of Io cooling and heating during eclipse and predictions of previous thermophysical theories. The radiance that the observations approached asymptotically after eclipse is much lower than the preeclipse value, an effect which has been noted before. We suggest that this difference is partly accounted for by the rotation of Io, which was not included in earlier theoretical models.

I. INTRODUCTION

A number of investigators have shown that observations of the thermal emission from Io during eclipse by Jupiter yields data from which the total thermal flux from the volcanoes can be estimated (Sinton et al., 1980; Morrison and Telesco, 1980; Matson et al., 1981; Sinton, 1981). The best published value for the total heat flux is 1.5 ± 0.3 W m^{-2} (Morrison and Telesco, 1980). Because this value is larger than most estimates of the heat produced by tidal dissipation (Yoder, 1979; Cassen et al., 1982; Greenberg, 1982; Yoder and Peale, 1981), it has been suggested that the heat flow from Io may be variable and that currently we are viewing an unusually high flux (Cassen et al., 1982; Pearl and Sinton, 1982; Sinton, 1982). Marked variability has been demonstrated at 4.8 μm (Sinton, 1983; Sinton et al., 1983). However, most of the heat flow is carried at wavelengths > 4.8 μm, and variability has never been demonstrated for this part of the spectrum.

One difficulty that is encountered in determining an accurate value of the total volcanic heat flux is the estimation and removal of the natural background of thermal emission from observations made during an eclipse. The thermal emission from the surface can be estimated for the time of lowest thermal emission (just prior to emergence from eclipse) by observing the rate of cooling of the surface at the beginning of the eclipse and the rate of warming after the eclipse and fitting theoretical models to these rates. However, the accurate estimation of the background contribution requires calculation of thermophysical models that include a number of effects that heretofore have not been included. The selection among these models must be made by comparison with good observations of the cooling and warming parts of the eclipse curve.

The spectrum of the thermal emission from the volcanoes is poorly known. For the most part, the spectrum has been observed in rather broad filters that insufficiently elucidate the spectral dependence. In addition, the spectrum of the emission from the volcanoes is unobservable beyond 30 μm because of the atmospheric cutoff. Even if these wavelengths were observable, the emission from the volcanoes may not be distinguishable from the normal thermal emission. These uncertainties in the spectrum lead to uncertainties in the value for the heat flow. One approach that has been taken for utilizing the available observations has been the proposal of a model for the emission from various parts of the volcanoes that include the active vents, the current flow activity, and the still-cooling old flows, and the determination of the spectrum from this model (Sinton, 1982). This model, which we shall call the flow model, has to be tested, however, before it can be confider_ly used to determine an accurate value for the heat flux.

It is with these aims in mind; i.e., testing the flux for variability, determining accurate models for the thermophysical cooling, and evaluating the spectrum of the volcanic emission, that we have observed a number of eclipses of Io in spectral bands between 3.5 and 30 μm. In this paper we present and discuss our observational data. In later papers we will discuss thermophysical models and application of the flow model to these data.

II. OBSERVATIONS

All observations reported here have been made with the Infrared Telescope Facility (IRTF) 3-m telescope on Mauna Kea and its bolometer system #1. Characteristics of the filters, taken from the Handbook of the IRTF, are given in Table I.

The list of filters actually used was modified through the first year. Initially, we sought to avoid using the very broadband 10.2-μm filter and opted for narrowband filters which included one at 7.9 μm and a special 0.2-μm-wide filter centered on a narrow window in the 6.3-μm H_2O band. Though we could make quite good measurements of standard stars with this latter filter, the S/N was not adequate for Io observations. We later standardized on narrow band filters at 8.7 and 12.5 μm but also included the broadband 10.2-μm filter because it required very little observing time and because its use was desired by others who are interested in these data.

Several standard objects have been observed during the course of these observations, α Boo, β Gem, μ UMa, and Callisto, and we have managed to obtain observations of two of these at each eclipse. The magnitudes for the stars used in the reductions are given as notes to Tables IIa and IIb. The zero-magnitude fluxes are taken from Beckwith et al. (1976). The calibration of Callisto will be discussed in a later section.

We used an aperture of 6-arcsec diameter. Chopping was of 10-arcsec amplitude and the direction was chosen to be perpendicular to the radius vector from Jupiter when Io was about 8 arcsec from the limb. It was anticipated that for an eclipse reappearance, Io could be acquired when it reached this distance at ~40 minutes prior to the reappearance. Offset coordinates to Io from other Galilean satellites were computed as a matter of course, and we had no trouble acquiring the eclipsed Io, even in daylight. Track rates were also computed and applied to the telescope drives to follow Io's motion. We first acquired Io using the 20-μm filter, which is the filter where the largest signal is obtained. The automatic centering program, provided at the IRTF, was used to peak the 20-μm signal. We repeated this centering operation every time that we cycled through the 20-μm filter, whether Io was eclipsed or not.

Either before or after obtaining the eclipse data, we made observations of the sky at the nearest position to Jupiter at which we observed. We subsequently made corrections for scattered light to our Io data from these sky observations. The largest of these corrections was ~20%. From several observations at different radial distances made at the first eclipse, we found that the sky corrections were entirely negligible after about 10 to 15 minutes of Io's motion away from Jupiter. Usually, we were only allotted 1-1/2 to 2 hours of telescope time at each eclipse for this program. We found that with ample planning and after doing a "dry run" on the full night that we had for the first eclipse, we could execute the observations with high efficiency. The "dry run" data have been used for studying the sky corrections.

The observations are presented in Tables IIa through IIf. Naturally, the course of the program did not always go as smoothly as just described, and some comments about specific problems are in order. For the second year's observing, we assigned priorities to observations in the different filters. The highest priority was given to 10.2 and 20 μm. The next rank of priority was accorded to 4.8, 3.5, and 30 μm. Lowest priority was accorded to the narrow 8.7- and 12.5-μm filters. Their usefulness, however, is greatest just before emergence because it is then that the satellite surface is coldest and the spectrum of the volcanic emission can best be determined. Hence we generally tried to obtain data in these filters shortly before emergence. Background thermal emission from Io is not significant in the 3.5- and 4.8-μm filters. Therefore, it does not matter when measurements are obtained in these so long as we obtain a measurement in eclipse to measure the volcanic emission and one out of eclipse to determine the additional reflected sunlight. Generally we had sufficient time during the total eclipse phase to observe in all of the filters, but the priorities were applied to the eclipse

whose data are in Table IId. Here clouds cleared away just 10 minutes before reappearance. We used the 10.2- and 20-μm filters. Of the next rank we used 4.3 but not 3.5 and 30 μm because more time is required for a significant observation at these wavelengths. At the eclipse of Table IIf, the 30-μm window was not open. No data are included in the tables for 3.5 μm for the second year although the data exist. At present we have no adequate calibration for the Io observations at this wavelength. The system sensitivity apparently has been improved with the result that α Boo is too bright to observe at 3.5 μm. We have Callisto data for calibration, but at the moment we have no reliable connection between Callisto and a standard star at this wavelength.

A problem arose with the observations of Table IIc. After the observations were made it was discovered that the equipment was not rigidly bolted to the telescope. We believe that the calibration with Callisto is valid since these data were taken without moving the telescope very far. The calibration using α Boo is consistent with the Callisto calibrations except at 10.2 μm. At 20 μm and at 30 μm, all of the eclipses observed in 1982, Tables IIc - IIf, have been calibrated solely by the Callisto observations for reasons explained in the next section.

III. OBSERVATIONS OF CALLISTO

Callisto was observed along with Io for each of the eclipses in Tables IIc through IIf. In addition, A. Tokunaga kindly made available to us observations of Callisto and α Boo that he made on 4 Mar 1982. In part we have used the Callisto data to test the accuracy of our calibration procedure, particularly since observations of Callisto at one wavelength can be related to those at another wavelength by simple theory. One important consideration

in using Callisto as a test object is that little rotational variation is expected for the thermally emitted radiation. This follows from the fact that the radiometric Bond albedo, A, is a mere 0.13 (Morrison, 1977). Since the thermally reradiated emission is proportional to 1-A, the emission can vary by only a few percent. Another important consideration in using Callisto is its relatively long rotation period of 16 days. The long period, when combined with its low value of thermal inertia, 2.4×10^{-4} cal cm^{-2} s$^{-1/2}$ K^{-1} (Morrison, 1977) means that every part of the illuminated surface is close to equilibrium with the insolation. As a consequence, the total of the distribution of emission over the surface can be treated by an integration which, as it turns out, can be performed in closed form.

The observational data for Callisto are presented in Table III. The first four rows of the table give the observed radiance at each wavelength averaged over the filter band width and where a radius of 2400 km has been assumed (Davies, 1982). For the broadband 10.2-, 20-, and 30-μm filters the monochromatic radiance must be computed. Mean Callisto radiances, given in row 5, have been corrected to monochromatic radiances by using Table 4 of Hansen (1972) for 10.2 and 20 μm and by similar calculations for 30 μm. We have assumed that the narrowband 8.7- and 12.5-μm filters are sufficiently monochromatic that no correction is necessary. The monochromatic fluxes are given in row 6. The brightness temperature, T_B, given in row 7, shows a noticeable trend toward lower brightness temperatures for longer wavelengths.

As mentioned above, it may be assumed that equilibrium prevails at every place on the sunlit side of Callisto, and hence the thermal emission is equal to the insolation. If, further, the Wien approximation is assumed, then the following equation must hold (Sinton, 1957):

$$\exp(-C_2/\lambda T_B) = 2\int_0^{\pi/2} \exp(-C_2/\lambda T_S \cos^{1/4}\theta) \sin\theta \cos\theta \, d\theta, \qquad (1)$$

where C_2 is the second radiation constant—14387 μm °K, λ is the wavelength, T_S is the subsolar temperature, and θ is the angle between the surface normal and the sun. For the worst case, at the subsolar point and at 30 μm, the Wien approximation is 5.6% too small. At 20 μm the maximum error is less than 2%. Since the Wien approximation is made on both sides of equation (1), the relative error in equation (1) is much less than these estimates. By a change of variable and by repeated integration by parts, the integral in equation (1) can be expressed as the exponential integral

$$\exp(-C_2/\lambda T_B) = e^x \sum_{n=0}^{7} n! \ x^{7-n} /7! - x^8 \ E_1(x)/7!, \qquad (2)$$

where $x = -C_2/\lambda T_S)$ and $E_1(x) = \int_x^\infty (e^v/v) \ dv.$

Equation (2) was solved for T_S by utilizing a routine giving six-digit accuracy for the exponential integral (Smith, 1975) and another routine which found the root for the difference of the two sides of the equation. The subsolar temperatures from these solutions are given in row 8 of Table III for the various wavelengths and observed brightness temperatures. The mean T_S, excluding the poorly determined 30-μm value, is 168.5° ± 0.7° K. We can use this subsolar temperature through equation (2) to calculate the expected T_B and from that determine the expected radiance. The expected radiance and the percentage difference of the observed value, row 6, from this are shown in rows 8 and 9 of Table III. The Callisto spectrum, calculated with T_S = 168.5° K, and the observed spectral data are shown in Figure 1. Except for 8.7 μm the differences between the observed and the calculated radiances are within observational uncertainties. Lastly, we can use the subsolar temperature to calculate the amount of flux being received from the sun and to compare this value with that expected. From Jones and Morrison (1974) we can write

$$A = 1 - (T_S/T_E)^4 R^2, \qquad (3)$$

where T_E is the equilibrium temperature of a black, nonconducting surface at the Earth's distance from the Sun, and R is the distance of Callisto from the Sun in AU (5.42 to 5.44 during the sequence of observations). Recent measurements of the solar constant (Frohlich, 1977) give T_E = 394.5° ± 1.5° K. With T_S = 168.5° K, A is 0.025 ± 0.023. Naturally, A is very poorly determined by equation (3) and may suffer from model deficiencies in the tacit assumption that the emissivity is unity and the assumption that the surface is smooth that is inherent in equation (1). However, the difference between 0.025 and the expected value of 0.13 signifies that the calibration by the stellar measurements is probably not in error by more than 10% when averaged over the observations on different nights and at different wavelengths. We estimate that for the Io observations the absolute calibration uncertainties are 10% or less at 8.7 μm, 10.2, 12.5, and 20 μm, and 15% at 30 μm.

For the data in Table IIc, where the α Boo measurements were deemed unreliable, we have used the mean Callisto radiances from Table III for wavelengths 8.7 through 20 μm. For 30 μm we have used the average of the one observed value in Table III and the calculated radiance based on T_S = 168.5° K.

If we look at the 20-μm Callisto radiances for individual nights in Table III, we discover that the 23 July and 14 June radiances are quite low. We know that 23 July was humid enough that the 30-μm window was not open, and 14 June was probably also humid because clouds had just disappeared. The atmospheric attenuation in the 20-μm filter band is much greater at the long wavelength end of the filter than at the shorter end. Yet a star, with a Rayleigh-Jeans spectrum, contributes most of its energy at the short wavelength end of the band. On the other hand, Callisto's and Io's energies

are rather uniformly distributed across the filter band. We have, therefore, adopted Callisto as the calibrator at 20 μm. We have also used it at 30 μm because the same problem exists at this wavelength. Adopting Callisto as the calibrator substantially reduced the scatter in the Io radiances at 20 μm when different eclipses were compared.

At 4.8 μm, where reflected sunlight dominates, Callisto does exhibit a rotational variation ~0.5 mag, a result that is based upon 14 nights of observations with the UH 2.2-m and IRTF telescopes. We have used the mean of two nights data obtained at rotational phase angles within 15° of its phase on 19 March 1982 to determine its brightness for calibration in the data presented in Table IIc.

IV. DISCUSSION OF THE IO ECLIPSE DATA

A result that can be obtained from the 4.8 μm data in the tables is a determination of the albedo of the Io surface that is free from contributions of emission. Differencing the means of the 4.8 μm radiances before and after reappearance, Tables IIa, IIb, IIe, and IIf, we find solar reflected radiances of 2.86, 2.79, 2.50, and 2.66 μW cm^{-2} sr^{-1} μm^{-1} with a mean of 2.70 ± 0.08 μW cm^{-2} sr^{-1} μm^{-1}. A white, lambert-reflecting surface at Io's distance from the Sun would reflect 3.90 μW cm^{-2} sr^{-1} μm^{-1}. Thus Io's albedo is 0.69 ± 0.02 at the orbital phase angle ~17° that is attained when eclipse reappearance occurs. For the disappearance data in Table IIa we similarly find an albedo of 0.53. From Sinton et al. (1980), Table 1, we quote values for three eclipse disappearances of 0.50, 0.64, and 0.71. The combined mean albedo is 0.60 ± 0.05 which applies to the orbital phase angle ~343° that is attained when disappearances occur. Both of these albedos apply to a solar phase angle ~9° when the observations were made. Sinton et al. (1983) found a linear

solar phase coefficient of -0.004 ± 0.005 mag degree^{-1}. If this very uncertain correction is applied, the geometric albedo (at solar phase = $0°$) may be 0.71 ± 0.04 and 0.62 ± 0.06 at $17°$ and $343°$ orbital phase angles, respectively.

We may compare these two values to the noneclipse determinations of the apparent geometric albedos, which include contributions of volcanic thermal emission, given in Sinton et al. (1983). Only 4 of the 173 values listed in this reference are comparable to the true albedo values found here. They are almost always much larger. Thus we conclude that thermal emission from volcanoes can be observed virtually all of the time at 4.8 μm.

The 10.2-μm radiances of Io are shown in Figure 2 and the 20-μm radiances are shown in Figure 3. The times in the figures are relative to the ephemeris times for disappearance or reappearance. The first thing to note from the data in the figures is that the disappearance and reappearances consistently occur about 3 minutes earlier than the ephemeris time.

We have also included Morrison and Telesco's (1980) data in these figures. Our 10.2-μm radiances are systematically lower by $\sim 0.0.2 \mu W$ cm^{-2} sr^{-1} μm^{-1} than their 1980 data. We do not know whether these differences represent a change in the Io volcanism or a difference in the calibration of their data relative to ours. We have used basically the same procedures, the same equipment, and for the most part the same calibration star. At 10 μm it is unusual to have a random error this large for sources as bright as Io and α Boo. We have also compared our 1982 preemergence measurements with the 1981 preemergence measurements and with Morrison and Telesco's measurements in the 10-μm window. The results of this comparison are shown in Figure 4. The mean of the preemergence 10.2-μm values for each eclipse are plotted in this figure as circles. We have also determined values for 10.2 μm by interpolating to

12.5 μm when these data are available. These are plotted as filled circles. The figure shows that the 10.2-μm radiance of Io is remarkably constant, but if a change has occurred since 1980, there most likely has been a decrease. A nominal uncertainty of 5% has been applied to each eclipse measurement. This is smaller than the 10% estimate by Morrison and Telesco (1980) as their estimate was mostly based on the uncertainty of the absolute flux calibration while for the discussion of variability only statistical errors are involved. The same type of comparison is made in Figure 5 for the 20-μm preemergence flux. The data in this figure show no evidence of a change. More than 90% of the flux at 10.2 μm and more than 60% of the flux at 20μm result from thermal emission from the volcanoes. Since these wavelengths are near to the peak of the volcanic flux, these results imply that there has been very little change in the total heat flux.

Figures 2 and 3 also exhibit a phenomenon that at this time is not completely understood. The flux levels at both 10.2 and 20 μm that are asymptotically approached after eclipse are well below those prior to the eclipse. This phenomenon was seen in much earlier data (Morrison, 1977, pp. 275, 277). Morrison suggested two causes for the effect: a) an additional heat sink is somehow introduced during the eclipse, and b) the albedo changes during the eclipse. We suggest a possibility that is really an elaboration of the first. During the more than two hours of the eclipse, Io rotates by 20° and night-cooled surface has been brought around to the sunlit side when the eclipse ends. Thus the chilled subsurface serves as a sink for the insolation, while some of the previously heated subsurface is rotated off of the disk. This statement may appear invalid because the rotation-caused sink exists before the eclipse begins and because the asymptotic flux after the

eclipse must be identical to the preeclipse flux. The last statement must be
strictly true if equilibrium is reached. But our model calculations for a
homogeneous surface with the required value for the thermal inertia show that
equilibrium is not reached during the diurnal variation. At the subsolar
point, about 10% of the insolation is still being conducted inward to fill the
sink left by the nighttime cooling. The loss of two hours of heating during
the eclipse adds to the nighttime deficit. Thus the loss of insolation by
inward conduction is greater after the eclipse than it was before it, and a
quasi-stable, but lower, surface temperature is reached an hour or two after
the eclipse.

An additional but small asymmetry in the observed out-of-eclipse thermal
emission is produced by the fact that eclipse disappearances are observed when
the subearth point is at a longitude ~9° toward afternoon, while the
reappearances are observed at a similar longitude toward morning. Preliminary
homogeneous models have been computed in which the surface of Io is divided
into 40 equal areas. The temperature structure is computed for each of these
areas for at least an entire day before the eclipse integration begins. In
our models, Io is rotated as the eclipse progresses. From our model
calculations, we believe that this explanation is a substantial part of the
effect. We are continuing these calculations with vertically and horizontally
inhomogeneous models. An additional part of the phenomenon may be caused by
albedo changes brought about by rotation since Io rotates by ~30° from the
beginning of the eclipse until full recovery. The known longitudinal albedo
variations (Johnson and Pilcher, 1977; Morrison, 1977; Sinton et al., 1983)
are such as to cause cooler posteclipse equilibrium temperatures than
preeclipse temperatures. Yet another part of the phenomenon may be a
variation of the volcanic heat flux brought about by rotation, i.e., the

average heat flux is not constant with longitude. We note from Figures 2 and 3 that there is a marked decrease of flux continually during the total phase of the eclipse. All eclipse cooling models that we have computed have much smaller slopes during the eclipse. An albedo variation cannot cause a significant slope because the albedo is not relevant during the eclipse. We believe that until the asymmetry of the eclipse thermal emission is completely understood, it is premature to derive a definitive value for the heat flow of Io. The next paper of this series will attempt to achieve a model that will fit both the disappearance and reappearance curves.

V. ACKNOWLEDGMENTS

REFERENCES

Beckwith, S., N. J. Evans, E. E. Becklin, and G. Neugebauer (1976). Infrared observations of Monoceros R2. Astrophys. J. 208, 390-395.

Cassen, P. M., S. J. Peale, and R. T. Reynolds (1982). Structure and thermal evolution of the Galilean satellites. In Satellites of Jupiter (D. Morrison, Ed.), pp. 93-128. Univ. of Arizona Press, Tucson.

Davies, M. E. (1982) Cartography and nomenclature for the Galilean satellites. In Satellites of Jupiter (D. Morrison, Ed.), pp. 911-933. Univ. of Arizona Press, Tucson.

Frohlich, C. (1977). Contemporary measures of the solar constant. In The Solar Output and its Variations (O. R. White, Ed.), pp. 93-109. Colorado Associated University Press, Boulder.

Greenberg, R. (1982). Orbital evolution of the Galilean satellites. In Satellites of Jupiter (D. Morrison, Ed.), pp. 65-92. Univ. of Arizona Press, Tucson.

Hansen, O. L. (1972). Thermal radiation from the Galilean satellites measured at 10 and 20 μm. Thesis: California Institute of Technology.

Johnson, T. V., and C. B. Pilcher (1977). Satellite spectrophotometry and surface compositions. In Planetary Satellites (J. A. Burns, Ed.), pp. 232-268. Univ. of Arizona Press, Tucson.

Jones, T. J., and D. Morrison (1974). Recalibration of the photometric method of determining asteroid sizes. Astron. J. 79, 892-895.

Matson, D. L., G. A. Ransford, and T. V. Johnson (1981). Heat flow from Io (J1). J. Geophys. Res. 86, 1664-1672.

Morrison, D. (1977). Radiometry of satellites and of the rings of Saturn. In Planetary Satellites (J. A. Burns, Ed.), pp. 269-301. Univ. of Arizona Press, Tucson.

Morrison, D., and C. Telesco (1980). Io: Observational constraints on the internal energy source and the thermophysics of the surface. Icarus 44, 226-233.

Pearl, J. C. and W. M. Sinton (1982). Hot spots of Io. In Satellites of Jupiter (D. Morrison, Ed.), pp. 724-755. Univ. of Arizona Press, Tucson.

Sinton, W. M. (1957). Spectroscopic evidence for vegetation on Mars. Astrophys. J. 126, 231-239.

Sinton, W. M. (1981). The thermal emission spectrum of Io and a determination of the heat flux from its hot spots. J. Geophys. Res. 86, 3122-3128.

Sinton, W. M. (1982). Io: A volcanic flow model for the hot spot emission spectrum and a thermostatic mechanism. Icarus 51, 563-573.

Sinton, W. M. (1983). On Io all that flickers is not cold. Submitted.

Sinton, W., A. Tokunaga, E. Becklin, I. Gatley, T. Lee, and C. Lonsdale (1980). Io: Ground-based observations of hot spots. Science 210, 1015-1017.

Sinton, W., F. Cheigh, D. Lindwall, and W. Tittemore (1983). Io: The near-infrared monitoring program, 1979-1981. Icarus, in press.

Smith, J. M. (1975). Scientific Analysis on the Pocket Calculator, pp. 116-121. Wiley-Interscience, New York.

Yoder, C. F. (1979). How tidal heating in Io drives the Galilean orbital resonance locks. Nature 279, 767-770.

Yoder, C. F., and S. J. Peale (1981). The tides of Io. Icarus 47, 1-35.

TABLE I

Characteristics of the Filters

Wavelength (μm)	Bandwidth (μm)
3.4	1.0
4.8	0.4
7.9	0.7
8.7	1.2
10.2	5.1
12.5	1.2
20	9
30	8

TABLE IIa

Io Reappearance 24 Apr 1981 UT

Calibration[a]: β Gem and α Boo

Reappearance: 7:17 UT

(Radiances $\mu W\ cm^{-2}\ sr^{-1}\ \mu m^{-1}$)

3.4 μm		4.8 μm		8.7 μm		10.2 μm		20 μm		30 μm	
Time	Rad.	Time	Rad.	Time	Rad.	Time	Rad.	Time	Rad.	Time	Rad.
7:09	0.24	7:11	0.74	7:06	1.92	7:00	1.56	7:13	3.19		
						7:15	1.71				
7:22	11.9	7:23	2.85	7:20	1.95	7:25	3.01	7:24	7.58	7:27	1.97
				7:29	2.04	7:34	3.52	7:32	8.54	7:36	2.50
				7:38	2.18	7:41	3.24	7:40	8.39	7:43	1.85
				7:46	1.86	7:51	3.65	7:48	7.24	7:52	1.98
				7:55	2.75	7:58	3.72	7:57	9.20	8:01	2.22
				8:03	2.67	8:07	3.65	8:05	8.70	8:08	1.80
				8:11	2.53	8:16	3.68	8:13	9.03	8:18	1.99
				8:20	2.57			8:22	9.20		
		9:24	3.65	9:54	2.87	9:46	3.86	9:44	11.7	9:47	3.62
9:58	15.2	10:02	3.55								

[a]Calibration magnitudes for β Gem: −1.16 at 3.4 μm, −0.97 at 4.8 μm, and −1.24 at 20 μm. For α Boo, they are −2.95 at 4.8 μm, −3.17 at 8.7 μm, −3.15 at 10.2 μm, and −3.30 at 20 and 30 μm.

TABLE IIb

Io Reappearance 11 Jul 1981 UT

Calibration[a]: μ UMa and α Boo

Reappearance: 4:23 UT

(Radiances $\mu W\ cm^{-2}\ sr^{-1}\ \mu m^{-1}$)

3.4 μm		4.8 μm		7.9 μm		12.5 μm		20 μm		30 μm	
Time	Rad.	Time	Rad.	Time	Rad.	Time	Rad.	Time	Rad.	Time	Rad.
3:57	0.11	3:59	0.72	3:52	1.23	3:55	2.36	3:45	3.65		
				4:13	1.03			4:01	3.46	4:03	3.00
4:19	0.45	4:21	2.26								
		4:22	3.45								
		4:23	3.58					4:26	7.36		

[a]Calibration magnitudes for μ UMa: -0.94 at 3.4 μm, -0.73 at 4.8 μm, -0.90 at 7.9 μm, -1.19 at 12.5 μm, and -1.20 at 20 μm. For α Boo, the same values as in Table IIa were used, with the addition of -3.12 at 7.9 μm and -3.33 at 12.5 μm.

TABLE IIc

Io Disappearance 19 Mar 1981 UT

Calibration: Callisto

Disappearance: 9:28 UT

(Radiances $\mu W \ cm^{-2} \ sr^{-1} \ \mu m^{-1}$)

4.8 μm		8.7 μm		10.2 μm		12.5 μm		20 μm		30 μm[a]	
Time	Rad.	Time	Rad.	Time	Rad.	Time	Rad.	Time	Rad.	Time	Rad.
				9:16	5.9			9:14	13.5	9:17	12.6
9:22	3.51			9:21	5.8			9:20	13.3		
9:29	1.30			9:28	3.95			9:27	9.7		
9:39	1.39			9:38	3.41			9:34	6.4	9:36	7.2
								9:42	6.0		
9:54	1.70	9:47	2.67	9:53	3.03	9:49	3.20	9:52	5.0		

[a]Note that these 30-μm data have a large uncertainty (~30%) because of the large air mass difference between the Io and Callisto observations.

TABLE IId

Io Reappearance 14 Jun 1982 UT

Calibration: α Boo and Callisto

Reappearance: 4:55 UT

(Radiances $\mu W\ cm^{-2}\ sr^{-1}\ \mu m^{-1}$)

4.8 μm		10.2 μm		20 μm	
Time	Rad.	Time	Rad.	Time	Rad.
		4:46	1.52		
4:53	1.25	4.50	1.34	4:52	2.23
5:00	2.99	4:56	2.44	4:58	6.88
		5:05	3.07	5:03	6.88
		5:06	3.15		
5:07	3.07	5:09	2.82	5:08	7.55
		5:14	3.30	5:12	8.20
		5:17	3.46	5:15	8.09
				5:18	8.91

TABLE IIe

Io Reappearance 14 Jul 1982 UT

Calibration: α Boo and Callisto

Reappearance: 7:04 UT

(Radiances $\mu W\ cm^{-2}\ sr^{-1}\ \mu m^{-1}$)

4.8 μm		8.7 μm		10.2 μm		12.5 μm		20 μm		30 μm	
Time	Rad.	Time	Rad.	Time	Rad.	Time	Rad.	Time	Rad.	Time	Rad.
		6:32	1.19	6:29	1.59			6:28	3.23	6:31	3.28
6:44	0.44					6:41	1.71	6:40	2.85		
6:53	0.45			6:48	1.43			6:47	3.09	6:49	2.63
		7:00	1.08	6:56	1.46	7:02	1.95	6:56	2.97	6:58	2.70
7:04	2.95										

TABLE IIf

Io Reappearance 23 Jul 1982 UT

Calibration: α Boo and Callisto

Reappearance: 3:28 UT

(Radiances $\mu W\ cm^{-2}\ sr^{-1}\ \mu m^{-1}$)

4.8 μm		8.7 μm		10.2 μm		12.5 μm		20 μm	
Time	Rad.	Time	Rad.	Time	Rad.	Time	Rad.	Time	Rad.
		2:54	1.31	2:51	1.42	2:56	1.89	2:50	3.38
3:04	0.41	3:08	1.24	3:06	1.38	3:09	1.37	3:20	2.68
3:13	0.35	3:18	1.18	3:17	1.37	3:20	1.43	3:16	2.85
3:23	0.32	3:28	1.46	3:27	1.60			3:26	3.14
3:31	3.02			3:34	2.75			3:33	7.17
				3:36	2.88			3:35	7.38
				3:40	2.99			3:40	7.94

TABLE III

Radiances and Temperatures of Callisto

Date (1982)	Radiances ($\mu W\ cm^{-2}\ sr^{-1}\ \mu m^{-1}$)				
	8.7 μm	10.2 μm	12.5 μm	20 μm	30 μm
4 Mar	6.0	14.3	20.6	32.8	
14 Jun		14.0		28.9	
14 Jul	6.3	15.8	26.3	36.5	17.5
23 Jul	5.9	13.1	22.2	24.8	
Mean, $\mu W\ cm^{-2}\ sr^{-1}\ \mu m^{-1}$	6.1 ± 0.1	14.3 ± 0.5	23.0 ± 1.7	30.7 ± 2.5	17.5
Monochromatic Rad. $\mu W\ cm^{-2}\ sr^{-1}\ \mu m^{-1}$	6.1 ± 0.1	11.1 ± 0.4	23.0 ± 1.7	32.2 ± 2.6	19.4 ± 2.9
T_B, K	156.4	153.6	154.8	151.2	146.8
T_S, K	169.7	167.3	169.5	167.3	163.7
Rad. (T_S=168.5) $\mu W\ cm^{-2}\ sr^{-1}\ \mu m^{-1}$	5.7	11.8	22.0	33.3	21.3
Obs-Comp., %	6.7	-6.0	4.4	-3.2	-9.1

FIGURE CAPTIONS

Fig. 1. The observed mean monochromatic radiances of Callisto from four nights are compared to the calculated radiance from equation (1) with a subsolar temperature of 168.5° K. The error bars for the 8.7-μm point are smaller than the symbol.

Fig. 2. Observations of Io eclipse disappearance and reappearance at 10 μm. Times are given relative to the ephemeris predicted time of disappearance or reappearance. The data of Morrison and Telesco (1980) are shown as circles. Our 1981 data are shown as points, and our 1982 data are shown as crosses. The curve is merely a smooth curve drawn to fit the experimental points.

Fig. 3. Observations of Io eclipse disappearance and reappearances at 20 μm. Symbols are the same as for Fig. 2.

Fig. 4. The preemergence 10-μm radiances are compared for the various eclipses including the one observed by Morrison and Telesco (1980). The open circles are data obtained i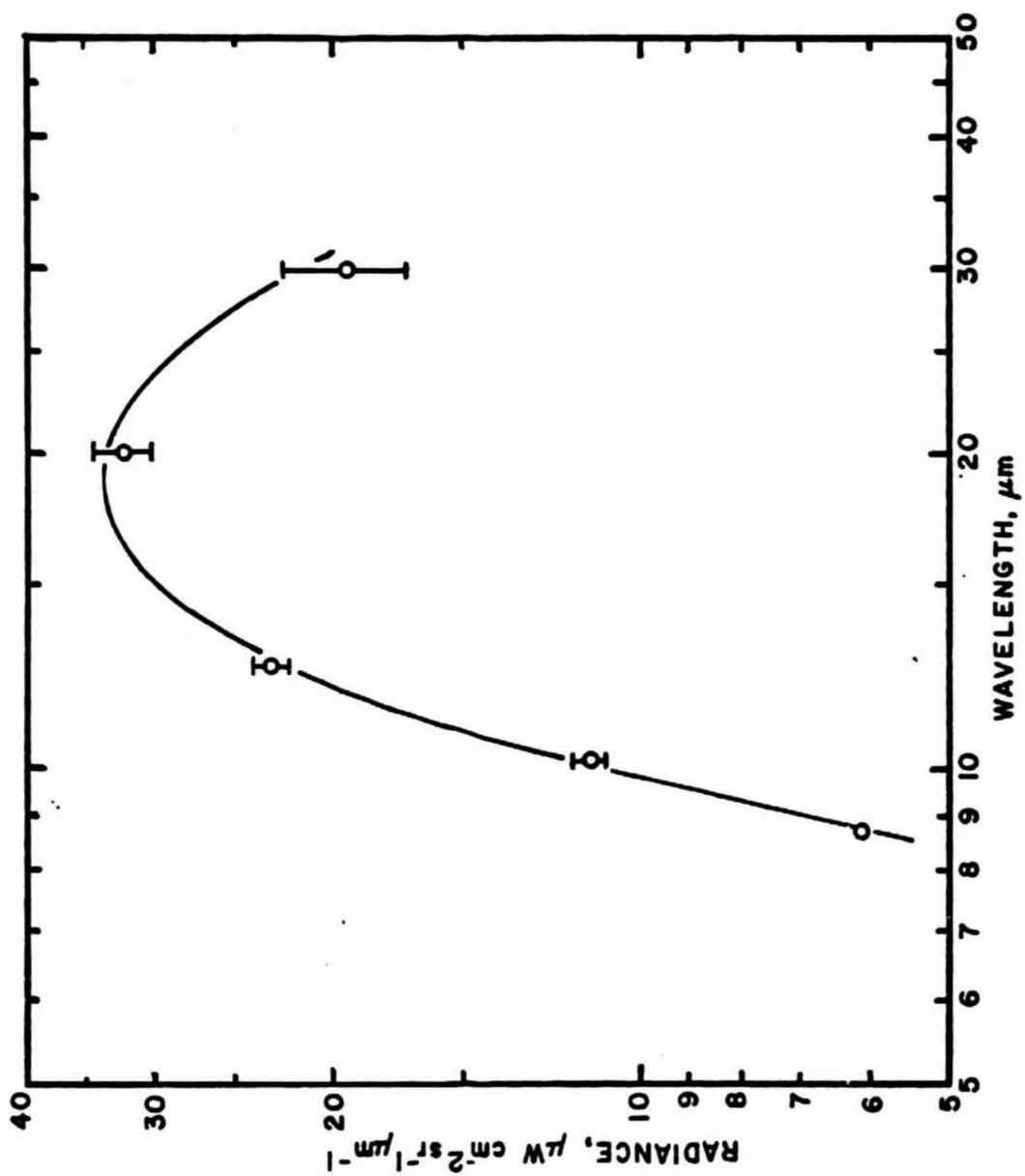n the 10.2-μm broadband filter. The solid points are obtained by interpolating to 10.2 μm the data from 7.9 and 12.5 μm.

Fig. 5. The preemergence 20-μm radiances are compared for the various eclipses, including the one observed by Morrison and Telesco (1980).

Fig. 1

Fig. 2

Fig. 3

Fig. 4

Fig. 5.